J Mater Sci (2007) 42:2735–2744
DOI 10.1007/s10853-006-1274-2

Effect of hot pressing time and temperature on the microstructure and mechanical properties of ZrB_2–SiC

Alireza Rezaie · William G. Fahrenholtz · Gregory E. Hilmas

Received: 18 July 2005 / Accepted: 26 January 2006 / Published online: 9 January 2007

Abstract Structure–property relations were examined for ZrB_2 containing 30 volume percent SiC particulates. Two grades of ZrB_2 with initial particle sizes of 2 and 6 μm were used. Billets of ZrB_2–SiC were produced by hot pressing at 1850, 1950 or 2050 °C for 45 min. In addition, the material prepared from ZrB_2 with an initial particle size of 2 μm was hot pressed at 2050 °C for 90 and 180 min. Microstructures and mechanical properties were characterized to determine the effects of the initial particle size, hot pressing time, and hot pressing temperature on the final grain size and morphology. The average grain size of the ZrB_2 phase ranged from 2.2 to 4.7 μm. Similarly, the average grain size of the SiC phase ranged from 1.2 to 2.7 μm. Hardness and modulus of elasticity were not affected by the processing conditions with average values of 22 and 505 GPa, respectively. However, flexural strength decreased as grain size increased from a maximum of ~1050 MPa for the finest grain sizes to ~700 MPa for the largest grain sizes. Analysis suggested that the strength of ZrB_2–SiC was limited by the size of the SiC inclusions in the ZrB_2 matrix.

Alireza Rezaie · William G. Fahrenholtz · Gregory E. Hilmas
Department of Materials Science and Engineering, University of Missouri-Rolla, Rolla, MO 65409, USA

Alireza Rezaie (✉)
Vesuvius Research, 4606 Campbells Run Road, Pittsburgh, PA 15220, USA
e-mail: alireza.rezaie@us.vesuvius.com

Introduction

Many modern designs for hypersonic flight vehicles and reusable atmospheric reentry vehicles incorporate sharp leading edges (radius as low as 1 mm) and smooth surfaces that may lead to smaller, lighter, and more maneuverable vehicles than ever before [1]. However, these design changes will lead to substantial increases in the temperatures encountered during use. For example, the heat flux at the leading edge increases inversely proportional to the square root of the leading edge radius; in other words, the leading edge temperature will increase as the radius decreases [2]. Whereas the maximum temperatures at the leading edge of the current space shuttle orbiter are ~1650 °C, leading edge temperatures of 2000 °C or above are expected for vehicles with sharp leading edges [3].

The high melting point of refractory metal diborides (>3000 °C) along with the ability to form refractory oxide layers gives these materials the capability of operating in oxidizing environments at temperatures of 2000 °C or above [4–6]. The diborides, including ZrB_2, have been considered for use in thermal protection systems and propulsion systems for hypersonic flight vehicles as well as thermal protections systems for re-entry vehicles [4, 7–12] In addition to the properties that make it attractive for aerospace applications, ZrB_2 is resistant to molten metals and slags, which has led to its use as a monolithic refractory material and as a protective sleeve in submerged entry nozzles for continuous steel casting [13–16]. Zirconium diboride is also reported to be highly resistive to plasma sparks and/or arcs which makes it suitable for high temperature electrodes in plasma applications [17].

The borides and carbides of the early transition metals, such as ZrB_2, ZrC, HfC, and TaC, are often referred to as ultra-high temperature ceramics (UHTCs). These materials have strong covalent bonding characteristics, low volatility, and high thermal and electrical conductivity [18]. Among UHTCs, ZrB_2 has the lowest theoretical density (6.09 g/cm^3), which makes it attractive for aerospace applications [12]. Combined with its high melting temperature, ZrB_2 is reported to have excellent resistance to thermal shock and oxidation compared to other non-oxide structural ceramics [12]. Often, SiC is added to ZrB_2 to enhance its oxidation resistance and limit grain growth during densification [4]. Additions of up to 30 volume percent SiC particulates were found to improve the four-point bend strength of ZrB_2 from ~565 MPa to ~1089 MPa and fracture toughness from 3.5 to 5.25 MPa m$^{1/2}$ by limiting grain growth and promoting crack deflection [6, 12]. For the study reported in this paper, a composition of 70 vol% ZrB_2 and 30 vol% SiC was selected based on previous studies that reported a combination of high four-point bend strength, improved fracture toughness, and enhanced oxidation resistance for this composition compared to materials with lower SiC contents [5, 6, 12].

Zirconium diboride-based ceramics can be prepared from commercial powders or synthesized using a variety of reaction based methods [5, 9, 19–22]. As with other non-oxide ceramics, ZrB_2 is usually densified by pressure assisted sintering techniques at very high temperatures (>1900 °C) [12]. The high densification temperatures alone can promote grain growth, which has been shown to reduce strength in other systems such as MgO and Al_2O_3 [23–25]. For ZrB_2, additions of Si_3N_4 [1] and SiC [1] or Fe [26] have been used to reduce the sintering temperature or the processing time, which can reduce the grain size and increase flexural strength. However, the addition of sintering aids often results in the formation of grain boundary phases that reduce strength at elevated temperatures [1, 12]. As an example, the strength of ZrB_2 containing ~3 volume percent Ni has been shown to drop by about 60% between 800 and 1000 °C [12].

The purpose of this article is to report the effect of grain size on hardness, modulus of elasticity, fracture toughness, and strength of ZrB_2 ceramics containing 30 volume percent SiC additions.

Experimental procedure

Processing

Two grades of commercially available ZrB_2 were used in this study. The smaller particle size ZrB_2 powder (Grade B, H.C. Starck, Newton, MA) had a purity of >99% (metals basis) and a reported starting particle size of 2 μm. The larger particle size powder (Grade A, H.C. Starck, Newton, MA) had a purity of >99% and a reported starting particle size of 6 μm. The SiC powder (Grade UF-10, H.C. Starck, Newton, MA) was predominantly α-SiC, and it had a reported purity of 98.5% and a particle size of 0.7 μm. Batches containing 70 vol% ZrB_2 and 30 vol% SiC were prepared. To reduce particle size and promote intimate mixing, the batches were attrition milled (Model 01-HD, Union Process, Akron, OH). For milling, a 750 ml fluoropolymer-coated bucket was charged with ~250 ml hexane, ~150 g of powder, and ~3000 g of Co-bonded WC milling media (~3.5 mm diameter). Powders were milled at 600 rpm for 2 h. To minimize segregation by sedimentation during drying, solvent removal was performed using rotary evaporation (Model Rotavapor R-124, Buchi, Flawil, Germany) at a temperature of 70 °C, a vacuum of 200 mmHg (~27 kPa), and a rotation speed of 150 rpm.

Milled powders were hot-pressed (Model HP-3060, Thermal Technology, Santa Rosa, CA) in graphite dies lined with graphite foil and coated with BN. Each of the different powder mixtures was hot-pressed at 1850, 1950 or 2050 °C for 45 min at a pressure of 32 MPa. In addition, the mixture prepared from ZrB_2 with an initial particle size of 2 μm was hot pressed at 2050 °C for 90 and 180 min at 32 MPa. After loading the powder into the dies, the furnace was heated at an average rate of ~10 °C/min to the hot pressing temperature. The powders were heated in vacuum (~150 mTorr) up to 1650 °C at which time the atmosphere was switched to flowing argon. A detailed description of the temperature ramp used to prepare the specimens has been reported previously [5]. Above ~800 °C, the temperature of graphite die was monitored using an infrared thermometer (Model OS 3708, Omega Engineering, Stanford, CT). When the die temperature reached the hold temperature, a uniaxial load of 32 MPa was applied. The furnace was cooled at ~20 °C/min to room temperature when the hot pressing time (45, 90, or 180 min) had elapsed. The load was removed when the die temperature dropped below 1750 °C.

Each billet was assigned a code to designate the grade of ZrB_2 (A or B), the hot-pressing temperature (1850, 1950, or 2050 °C), and the hot-pressing time (45, 90, or 180 min) as summarized in Table 1. Two billets were prepared for each combination of ZrB_2 grade, hot pressing temperature, and hot pressing time. Each billet had a diameter of ~40 mm and thickness of ~5 mm.

Table 1 Combinations of ZrB_2 type, hot pressing temperature, and hot pressing time

Material	ZrB_2 grade	Temperature (°C)	Time (min)	Abbreviation
ZrB_2–SiC (30 vol%)	A	1850	45	A-1850-45
ZrB_2–SiC (30 vol%)	A	1950	45	A-1950-45
ZrB_2–SiC (30 vol%)	A	2050	45	A-2050-45
ZrB_2–SiC (30 vol%)	B	1850	45	B-1850-45
ZrB_2–SiC (30 vol%)	B	1950	45	B-1950-45
ZrB_2–SiC (30 vol%)	B	2050	45	B-2050-45
ZrB_2–SiC (30 vol%)	B	2050	90	B-2050-90
ZrB_2–SiC (30 vol%)	B	2050	180	B-2050-180

Characterization

The bulk density of each billet was measured using the Archimedes technique with deionized water as the immersing medium. The reported density for each processing condition is the average value from the measured bulk density of the two billets prepared at that condition. To determine the relative density, the bulk density was divided by the true density. The true density of the billets was slightly higher than expected based on the ZrB_2:SiC ratio due to the incorporation of an unknown amount of WC into the batches during milling and the loss of an unknown amount of volatile material during hot pressing. Thus, it was necessary to measure the true density of each hot pressed billet. True density was determined by grinding a small amount (~5 g) of material to –325 mesh to expose as much of the closed porosity as possible and then performing helium pycnometry (Model 1305 Multivolume, Micromeritics Instrument Corp., Norcross, GA). The microstructure of each billet was characterized using scanning electron microscopy (SEM; S—570, Hitachi, Tokyo) along with energy dispersive spectroscopy (EDS; AAT, X-ray Optics, Gainesville, FL) for chemical analysis. Samples were prepared for microscopy by cutting cross sections parallel to the hot-pressing direction and then polishing to a 0.25 μm finish using diamond abrasives. Polished sections were thermally etched at 1550 °C for 30 min in a graphite resistance heated furnace (Model 1000-3060-FP20, Thermal Technology, Santa Rosa, CA). Grain sizes were determined using Image J (ImageJ, US National Institutes of Health, Bethesda, MD) by counting a minimum of 250 grains. The average of the longest and shortest diameter of the grain was reported as the grain size.

Mechanical testing

Hardness was determined by Vickers indentation (Model V-1000-A2, Leco, St. Joseph, MI) using a load of 300 g and a dwell time of 30 s. Reported values were obtained from an average of 20 indentations on a single specimen. Modulus of elasticity was measured using impulse excitation (Model MK4-I Grindosonic, J.W. Lemmens, St. Louis, MO) according to ASTM Standard C1259 [27]. At least 10 measurements from various bars cut from the two hot pressed billets were averaged to obtain the reported value for each processing condition. Flexural strengths were measured in four-point bending using a fully articulated test fixture according to ASTM Standard C1161 for type-A bars (25 mm by 2 mm by 1.5 mm) [28]. Between 9 and 12 bars (randomly selected from the two billets for each processing condition) were fractured for each processing condition to determine the reported averages and standard deviations. Finally, fracture toughness was determined by fracturing five samples in four-point bending after Vickers indentation [29]. A load of 10 kg was used to produce radial-median cracks before bend testing. Toughness was calculated according to the method described by Wachtman [30].

Results and discussion

Density

The measured bulk densities ranged from 5.22 to 5.35 g/cm^3 (Table 2). Using a simple rule of mixtures and assuming true densities of 6.09 g/cm^3 for ZrB_2 and 3.21 g/cm^3 for SiC, the theoretical density of ZrB_2 containing 30 vol% SiC should be 5.23 g/cm^3. The measured bulk densities were generally higher than the predicted true density due to the introduction of WC during attrition milling. As a result, true density was measured for each hot pressed billet to calculate its relative density. Using the measured true densities, the relative densities ranged from ~97 to nearly 100%, with all but one relative density more than 98%. Assuming that the increase in density was due to WC incorporation, the WC content of each material was estimated from the measured true densities using a rule of mixture calculation that assumed the true density of ZrB_2–SiC to be 5.23 g/cm^3 and the true density of the Co-bonded WC from the milling media as 14.96 g/cm^3. Using this

Table 2 Measured and calculated densities and WC content

Material	Archimedes density (g/cm^3)	True density (g/cm^3)	Relative density (%TD)	WC content (%vol)
A-1850-45	5.28	5.30	99.5	0.80
A-1950-45	5.29	5.39	98.2	1.67
A-2050-45	5.30	5.40	98.1	1.80
B-1850-45	5.22	5.37	97.2	1.47
B-1950-45	5.34	5.39	99.0	1.71
B-2050-45	5.32	5.33	>99.9	1.07
B-2050-90	5.33	5.41	99.0	1.93
B-2050-180	5.35	5.38	99.5	1.64

method, calculated WC contents were less than two volume percent in hot pressed samples. X-ray diffraction analysis (not shown) of milled and sintered materials showed that WC peaks were present after milling, but were absent after sintering. During hot pressing, WC is thought to react with ZrO_2 present on the surface of ZrB_2 as an impurity to form ZrC and W, both of which can dissolve into ZrB_2 and form a solid solution [31].

Modulus of elasticity, hardness, and fracture toughness

Elastic constant values of hot pressed materials varied from ~501 to 516 GPa, a range of less than 3%, with no apparent trend related to precursor particle size or processing conditions (Table 3). The average value of the modulus of elasticity for the entire population of the specimens was 506 ± 4 GPa. The measured values are slightly higher than rule of mixture predictions based on reported moduli of ZrB_2 (~500 GPa) [5, 32] and SiC (~475 GPa) [33]. The values of modulus are another indication that the hot pressed billets had high relative density since modulus decreases rapidly as porosity increases [30]. Likewise, hardness did not vary significantly with processing conditions and the average value was 22.0 ± 0.9 GPa for all processing conditions. Modulus of elasticity and hardness are inherent properties and they were not expected to vary significantly for the range of grain sizes produced for this study.

In contrast to modulus and hardness, fracture toughness varied slightly with the processing conditions (Table 3). The toughness appeared to vary with the starting particle size of the ZrB_2 powder, even though the powders were milled prior to hot pressing. For specimens prepared from the larger particle size ZrB_2, fracture toughness increased from ~3.9 MPa m$^{1/2}$ to ~4.3 MPa m$^{1/2}$ as hot-pressing temperature increased from 1850 to 2050 °C. For specimens prepared from the smaller particle size ZrB_2, fracture toughness decreased from ~5.5 MPa m$^{1/2}$ to ~ 4.3 MPa m$^{1/2}$ as hot-pressing temperature increased from 1850 to 2050 °C. Fracture toughness varied by less than ± 0.2 MPa m$^{1/2}$ when hot-pressing time increased from 45 to 180 min at 2050 °C.

To understand how the variations in fracture toughness related to microstructure, the specimens with the highest (5.5 MPa m$^{1/2}$) and lowest (4.2 MPa m$^{1/2}$) fracture toughness prepared from the finer ZrB_2 precursor were indented using a load of 10 kg and the paths of the indentation cracks were observed. From the SEM images of polished sections shown in Fig. 1, the indentation crack path in B-1850-45 appeared more tortuous than the crack path in B-2050-90. The more tortuous crack path is a qualitative indication that more energy was absorbed during crack propagation, which led to the higher measured toughness value for B-1850-45. Examination of crack paths on a thermally etched surface for B-2050-90 revealed that the fracture was transgranular, in most cases, and that crack deflection occurred near the SiC particles or at ZrB_2–SiC interfaces (Fig. 2).

Table 3 Measured modulus of elasticity, hardness, fracture toughness, and four point bend strength for ZrB_2–30% SiC

Material	E (GPa)	H (GPa)	K_{IC} (MPa m$^{1/2}$)	σ (MPa)	Number of strength bars
A-1850-45	503 ± 6	22 ± 2	3.9 ± 0.1	888 ± 151	9
A-1950-45	501 ± 1	22 ± 2	4.0 ± 0.2	770 ± 133	11
A-2050-45	503 ± 1	23 ± 2	4.3 ± 0.2	720 ± 38	9
B-1850-45	516 ± 3	20 ± 2	5.5 ± 0.3	1063 ± 91	10
B-1950-45	507 ± 3	22 ± 2	5.2 ± 0.4	1060 ± 59	11
B-2050-45	505 ± 2	23 ± 1	4.3 ± 0.2	854 ± 88	11
B-2050-90	508 ± 4	22 ± 1	4.2 ± 0.1	850 ± 100	11
B-2050-180	505 ± 1	22 ± 1	4.5 ± 0.2	804 ± 73	12

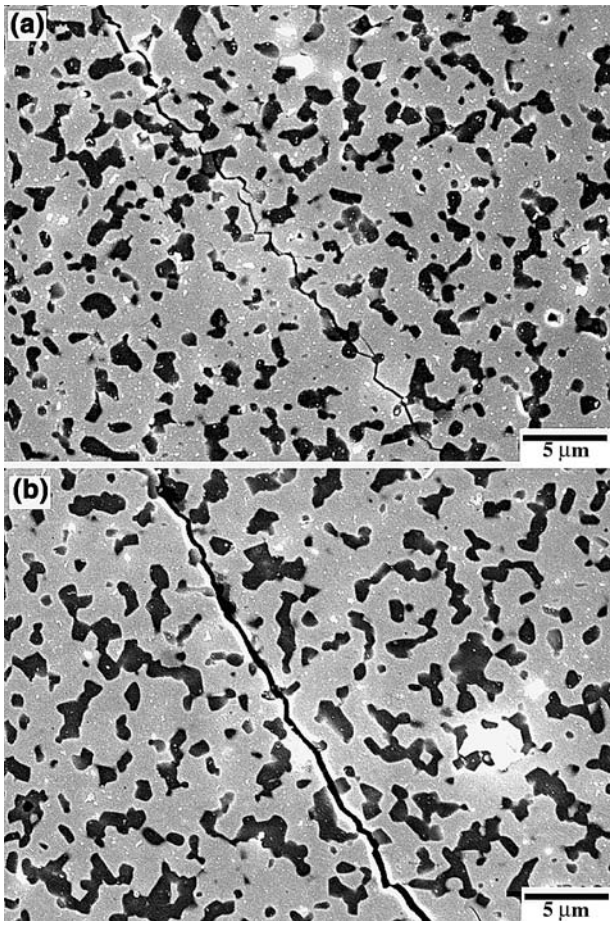

Fig. 1 Polished cross sections with indentation crack paths for the specimens with the (**a**) highest (5.5 MPa $m^{1/2}$ for B-1850-45) and (**b**) lowest (4.2 MPa $m^{1/2}$ for B-2050-90) fracture toughness of the specimens prepared from ZrB_2 with the finer starting particle size

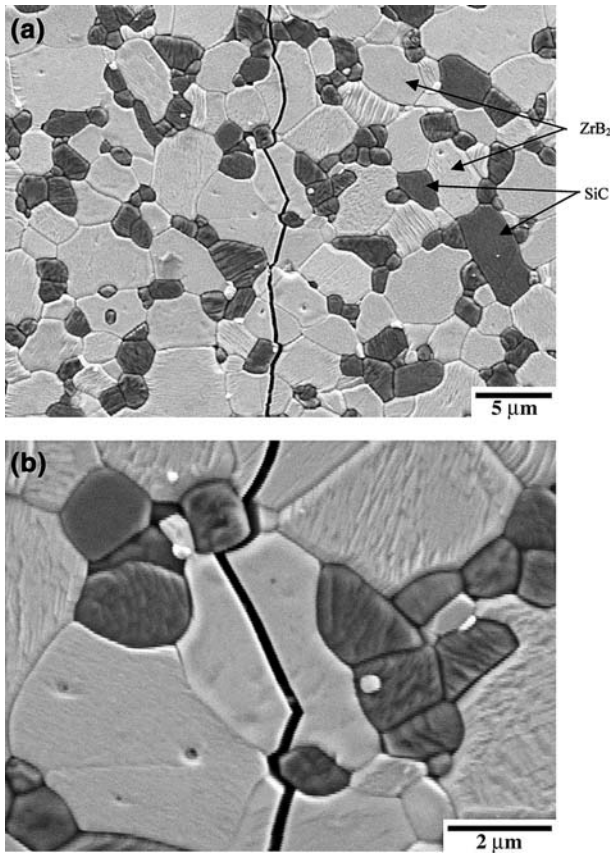

Fig. 2 A thermally etched cross section with an indentation crack path for B-2050-90 at (**a**) low and (**b**) high magnification showing crack deflection near SiC particles and predominantly transgranular fracture for ZrB_2

$$K(\theta) = K_{IC}(\theta = 0)\sec^2(\theta/2) \quad (1)$$

where: $K(\theta)$ is the measured fracture toughness (with crack deflection) in MPa $m^{1/2}$
$K_{IC}(\theta = 0)$ is the expected fracture toughness with no crack deflection in MPa $m^{1/2}$
θ is the crack deflection angle

Thus, the toughness of ZrB_2–SiC appears to be controlled by the size and distribution of the SiC particulates in the ZrB_2 matrix. The interactions of the indentation crack with the microstructure are most likely controlled by the complex residual stress state that develops during cooling from the processing temperature due to the thermal expansion mismatch between ZrB_2 (coefficient of thermal expansion 7–8 ppm/°C [32]) and SiC (CTE 3–4 ppm/°C [33]). Similar variations in fracture behavior have been reported for SiC reinforced alumina ceramics, which have similar thermal expansion characteristics to ZrB_2–SiC [34].

After the initial crack path observations, three specimens were selected for more detailed analysis. The model proposed by Wiederhorn (Eq. 1) was employed to investigate whether the increase in fracture toughness could be attributed to crack deflection [35]

The average and median values for the angle of crack deflection for each specimen were calculated by measuring at least 20 deflections (Table 4). The angles of deflection were determined by calculating the angle between each line segment of the crack, and the average direction of propagation of the crack. The average crack deflection angles ranged from about 22° (A-1850-45) for the lowest toughness material to about 50° for the highest toughness material (B-1850-45). These data clearly show qualitative agreement between increased fracture toughness and increased median or average crack deflection angle.

The measured fracture toughness values and the average deflection angles were used to calculate $K_{IC}(\theta = 0)$ values for the three specimens. It was

Table 4 Calculated $K_{IC}(\theta = 0)$ from K_{IC} and crack deflection angle

Material	K_{IC} (MPa $m^{1/2}$)	Median deflection angle	Average deflection angle	Number of crack deflections/mm	$K_{IC}(\theta = 0)$ (MPa $m^{1/2}$)
A-1850-45	3.9	22	25	~166	3.7
B-1850-45	5.5	48	50	~568	4.5
B-2050-90	4.2	40	39	~241	3.7

expected that all three specimens would have the same $K_{IC}(\theta = 0)$ because they all had the same composition. It was found that A-1850-45 and B-2050-45 had $K_{IC}(\theta = 0)$ values of ~3.7 MPa $m^{1/2}$, which were nearly identical to the fracture toughness of 3.5 MPa $m^{1/2}$ measured for pure ZrB_2 prepared by the same hot pressing procedure as used in the present work [12]. However, B-1850-45 had a significantly higher $K_{IC}(\theta = 0)$ value of ~4.5 MPa $m^{1/2}$. The model assumes that crack deflection is the dominant mechanism for increasing the fracture toughness. Therefore, if another mechanism such as crack twisting [35], crack bridging [36], matrix microcracking, or crack branching is active, then the model predictions would not be accurate [37, 38]. The crack paths examined by SEM (Figs. 1 and 2 as well as others) do not indicate a change in mechanism. However, the SEM observations do show a significant difference in the number of crack deflections observed per unit length of crack in B-1850-45 compared to the other two materials (Table 4). Based on both the Wiederhorn model calculation and the microstructural observations, it seems possible that the higher $K_{IC}(\theta = 0)$ of B-1850-45 is due to the increased number of deflections.

Strength

As with fracture toughness, the four point bend strength varied significantly with the processing conditions (Fig. 3). For specimens prepared from the larger particle size ZrB_2, strength decreased from ~890 MPa to ~720 MPa as hot-pressing temperature increased from 1850 to 2050 °C. Likewise, for specimens prepared from the smaller particle size ZrB_2, strength decreased from ~1060 MPa to ~850 MPa as hot-pressing temperature increased from 1850 to 2050 °C. Specimens prepared from the smaller particle size ZrB_2 showed a slight reduction in strength from ~850 MPa to ~800 MPa as hot-pressing time increased from 45 to 180 min. Closer examination of strength as a function of hot pressing time revealed that the observed decrease (~50 MPa) was not statistically significant compared to the standard deviations reported for the strengths (up to ~150 MPa).

The different materials were analyzed to understand how the variations of strength as a function of processing conditions related to their microstructures. Previous research has attributed some of the strength increase observed for ZrB_2–SiC compared to phase-pure ZrB_2 to the residual stresses that develop due to the CTE mismatch between the two constituents [5]. In this study, all of the specimens contained 30 volume percent SiC, so SiC content was eliminated as a variable. All of the specimens were hot pressed to near theoretical density, so porosity should not have a significant effect on strength. With no apparent change in fracture behavior, the strength variations observed in the materials were initially thought to be due to differences in ZrB_2 grain size. Fracture strength should increase as grain size decreases when other sources of flaws (machining damage during specimen preparation, porosity, etc.) are eliminated or minimized. The Griffith criterion (Eq. 2) states the fracture strength of a brittle

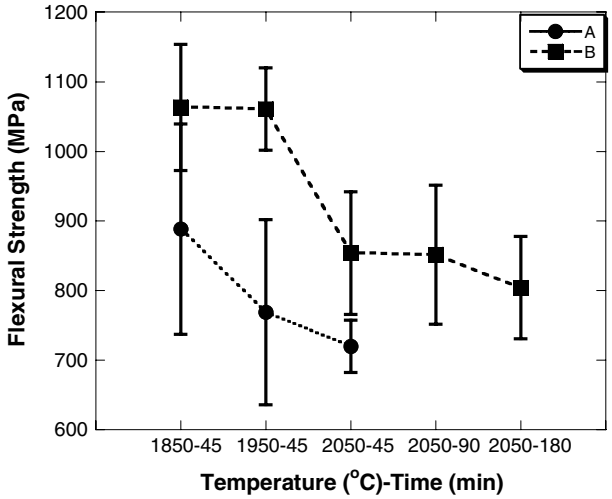

Fig. 3 Four point bend strength as a function of hot pressing time and temperature for ZrB_2–30% SiC prepared from the ZrB_2 powders with the fine (Grade B) and the coarse (Grade A) starting particle sizes

material is inversely proportional to the square root of its critical flaw size [30]

$$\sigma_{\text{fracture}} = \frac{K_{\text{IC}}}{Ya^{1/2}} \quad (2)$$

where: σ_{fracture} is the fracture strength in MPa
K_{IC} is the fracture toughness in MPa $m^{1/2}$
Y is a constant related to the fracture origin
a is the size of the strength limiting flaws in the material in meter

Average grain sizes were measured from thermally etched surfaces of each specimen (Figs. 4 and 5). For specimens prepared from ZrB_2 with the larger starting particle size, the average ZrB_2 grain size increased from ~2.1 μm to ~3.7 μm when hot pressing temperature increased from 1850 to 2050 °C. This was accompanied by a decrease in average strength from ~890 MPa to ~720 MPa (Fig. 6). Similarly, the average

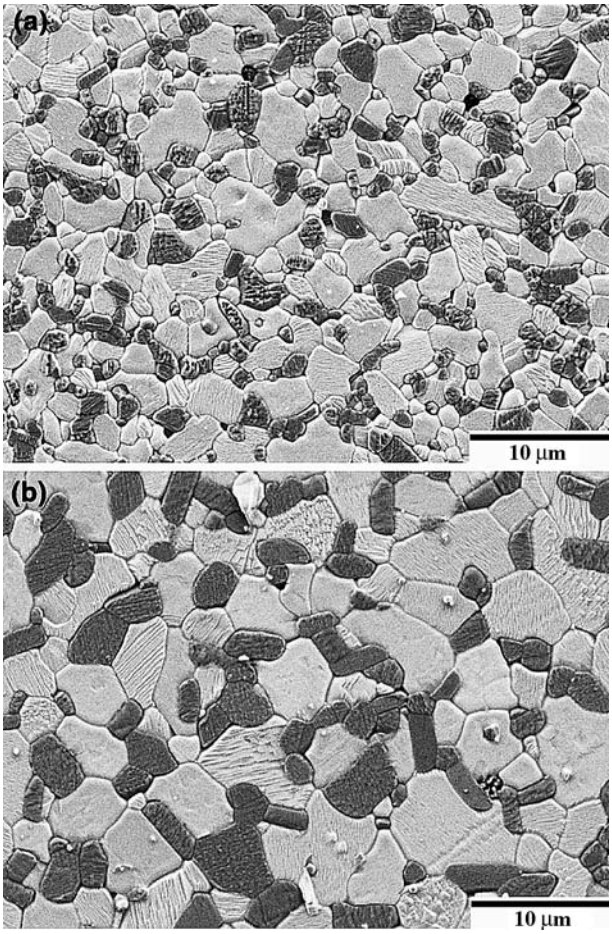

Fig. 4 Thermally etched surface microstructure of specimens prepared from larger starting particle size ZrB_2 hot pressed at (**a**) 1850 °C and (**b**) 2050 °C for 45 min

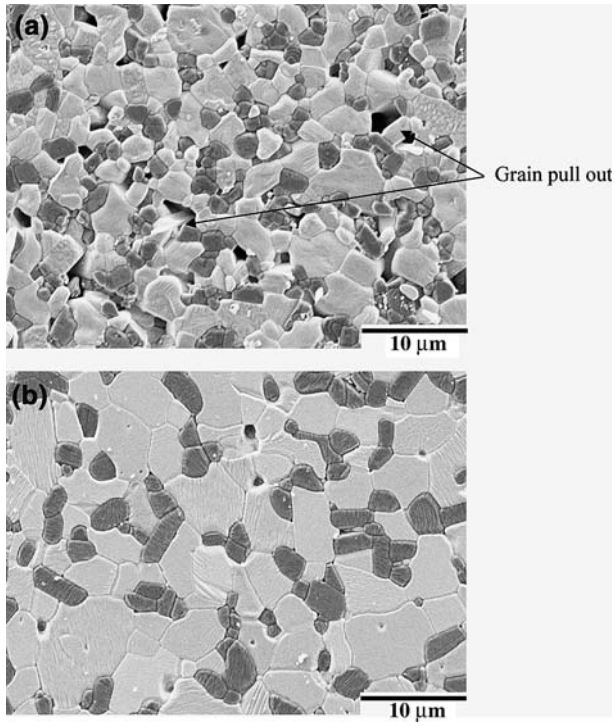

Fig. 5 Thermally etched surface microstructure of specimens prepared from smaller starting particle size ZrB_2 hot pressed at (**a**) 1850 °C and (**b**) 2050 °C for 180 min

ZrB_2 grain size increased from ~2.2 μm to ~3.5 μm for the specimens prepared from the smaller starting particle size ZrB_2 under the same conditions, which was accompanied by a decrease in strength from ~1060 MPa to ~850 MPa. In addition, the average ZrB_2 grain size increased from ~3.5 μm to ~4.7 μm, when hot pressing time increased from 45 to 180 min at

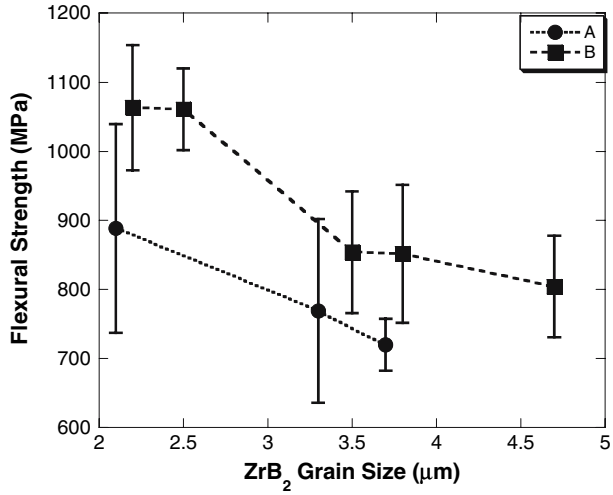

Fig. 6 Flexural strength as a function of the average ZrB_2 grain size

Table 5 Measured grain sizes and calculated critical flaw sizes for ZrB_2–30% SiC

Material	Ave. ZrB_2 grain size (μm)	Max. ZrB_2 grain size (μm)	Ave. SiC grain size (μm)	Max. SiC grain size (μm)	Critical flaw size (μm)
A-1850-45	2.1 ± 1.3	7.6	1.5 ± 0.7	3.8	5.0
A-1950-45	3.3 ± 1.5	12.4	2.5 ± 1.1	6.4	7.0
A-2050-45	3.7 ± 1.5	11.1	3.1 ± 1.3	8.7	9.1
B-1850-45	2.2 ± 1.2	6.5	1.2 ± 0.6	3.5	6.8
B-1950-45	2.5 ± 1.8	6.0	1.7 ± 0.8	5.4	6.0
B-2050-45	3.5 ± 2.0	8.2	2.0 ± 0.8	4.8	6.4
B-2050-90	3.8 ± 2.0	10.9	2.3 ± 0.9	6.0	6.3
B-2050-180	4.7 ± 3.0	20.9	2.7 ± 1.0	8.0	8.0

temperature of 2050 °C for specimens prepared from the smaller particle size ZrB_2. This increase in grain size was accompanied by a decrease in strength from ~850 MPa to ~800 MPa. Plotting strength as a function of the average ZrB_2 grain size (Fig. 6) suggests that the materials prepared from each type of ZrB_2 starting powder followed a Griffith-type model since strength decreased as the ZrB_2 grain size increased. However, materials with similar ZrB_2 grain sizes that were prepared from the different precursors had different strengths. For example, A-1850-45 and B-1850-45 had similar average ZrB_2 grain sizes (2.1 and 2.2 μm, respectively), but significantly different strengths (890 and 1060 MPa, respectively). This apparent contradiction led to a more detailed analysis of the critical flaw sizes.

The first step in the more detailed analysis was to determine the average SiC grain size for all of the materials. Then, the maximum ZrB_2 and SiC grain sizes were measured. The grain size data are compiled in Table 5. Only one SiC precursor powder was used for this study. Accordingly, the initial assumption was that SiC grain size would be similar for all materials and would not vary with hot pressing time and temperature since SiC particles were dispersed in a ZrB_2 matrix. However, analysis of SEM images showed that the SiC grain size varied from as low as 1.2 μm (B-1850-45) to as high as 3.1 μm (A-2050-45). Since the average starting SiC particle size was reported to be 0.7 μm, some SiC grain growth occurred in all of the specimens. For specimens prepared from the larger starting particle size ZrB_2, the SiC grain size doubled from ~1.5 μm to ~3.1 μm when hot pressing temperature increased from 1850 to 2050 °C. Likewise, the average SiC grain size increased from ~1.2 μm to ~2.0 μm for the specimens prepared from the smaller starting particle size ZrB_2 under the same conditions. The SiC grain size increased from ~2.0 μm to ~2.7 μm, when hot pressing time increased from 45 to 180 min at temperature of 2050 °C for the specimens prepared from the smaller particle size ZrB_2.

Plotting the four point bend strength as a function of the average SiC grain size resulted in an improved correlation between strength and feature size (Fig. 7), suggesting that the average size of the SiC grains was a factor in determining the strength of the ZrB_2–SiC. However, the two ZrB_2–SiC specimens prepared from Grade B powder with the finest average SiC grain sizes (B-1850-45 and B-1950-45) still did not seem to fit the trend shown by the other specimens.

To determine which microstructural features were most likely to act as the strength limiting flaws in ZrB_2–SiC, the average and maximum ZrB_2 and SiC grain sizes were plotted for each time–temperature combination for each of the ZrB_2 precursor powders (Fig. 8). In addition, the critical flaw size, a_{cr}, was calculated using the measured strength and fracture toughness values for each processing condition (Table 5) and Eq. 2. The calculated critical flaw sizes that had been calculated from the measured strength and toughness were also plotted as a function of the processing conditions for each ZrB_2 precursor. From Fig. 8, the critical flaw size was nearly identical to the maximum SiC grain size for all of the processing conditions.

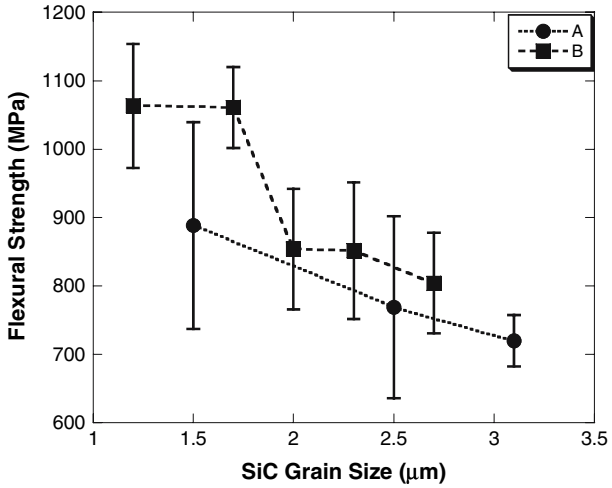

Fig. 7 Flexural strength as a function of the average SiC grain size

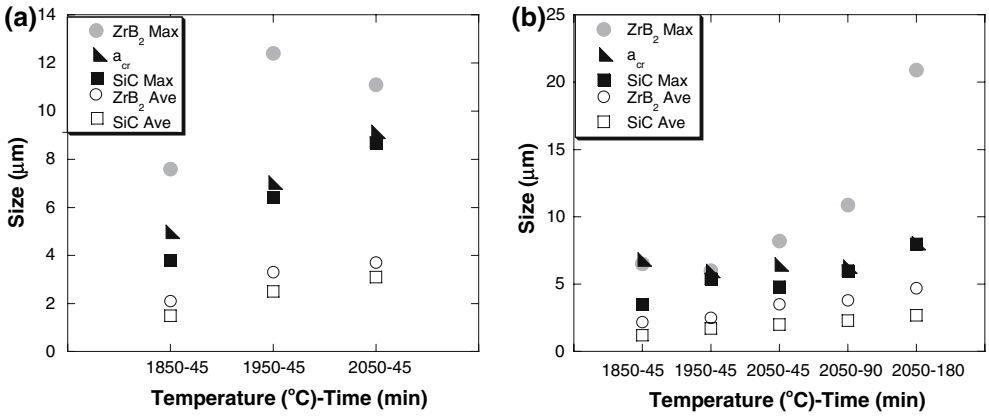

Fig. 8 Calculated critical flaw sizes (a_{cr}) compared to the average and maximum ZrB_2 and SiC grain sizes for ZrB_2–SiC prepared from (**a**) Grade A and (**b**) Grade B ZrB_2 precursors

The only specimen that showed significant deviation was B-1850-45, which had a calculated critical flaw size that matched more closely with the maximum ZrB_2 grain size than the maximum SiC grain size. This observation may indicate that strength is controlled by the maximum size of the ZrB_2 grains at below some critical SiC grain size, an assertion that is the subject of a continuing investigation. Based on the strong correlation between the critical flaw size calculated from measured strength and toughness and the microstructural observations, the strength limiting flaws in the ZrB_2–SiC materials examined in this study appear to be the largest SiC grains formed during hot pressing. This conclusion is consistent with the supposition from the earlier research attributing part of the strength increase that results from SiC additions to the residual stresses that develop due to the CTE mismatch.

Summary

Billets of ZrB_2 containing 30 volume percent SiC particulate additions were produced by hot pressing two different grades of commercial ZrB_2 powders. Analysis by SEM revealed a uniform dispersion of SiC particulates in the ZrB_2 matrix of all of the materials. Hardness and elastic modulus were not affected by different processing conditions and showed an average value of ~22 and 505 GPa, respectively. In contrast, fracture toughness and strength were found to depend on hot pressing temperature as well as the initial particle size of the ZrB_2 precursor. Fracture toughness values were analyzed using a model that suggested that the size and distribution of SiC could potentially affect toughness by altering the amount of crack deflection. Likewise, strength was also affected by the microstructure, specifically the grain size. Specimens prepared from the ZrB_2 powder with the smaller initial particle size had the highest strength (~1060 MPa) when hot pressed at 1850 °C for 45 min, which produced an average ZrB_2 grain size of ~2.2 μm and SiC grain size of ~1.2 μm. Increasing the hot pressing temperature to 2050 °C and the hot pressing time to 180 min for the same material resulted in an average ZrB_2 grain size of ~4.7 μm, SiC grain size of ~2.7 μm, and a strength of ~800 MPa. For samples prepared from the ZrB_2 with the larger initial particle size, the highest strength (~890 MPa) was obtained for hot pressing at 1850 °C for 45 min, which produced an average ZrB_2 grain size of ~2.1 μm and SiC grain size of ~1.5 μm. The lowest strength (~720 MPa) was obtained at 2050 °C for 45 min with the average ZrB_2 grain size of ~3.7 μm and SiC grain size of ~3.1 μm. Grain size was the critical factor determining the strength. Specifically, analysis suggested that the largest SiC grains in the microstructure acted as the critical flaw causing the failure of the specimen. Hence, smaller SiC grain sizes would result in even higher strengths for ZrB_2–SiC.

Acknowledgements This work was supported by the National Science Foundation on Grant DMR-0346800. The use of the Advanced Materials Characterization Laboratory at UMR is gratefully acknowledged. In particular, the authors would like to thank Dr. Scott Miller of the AMCL for his assistance.

References

1. Monteverde F, Bellosi A (2004) Adv Eng Mater 6:331
2. Kolodziej P. Aerothermal performance constraints for hypervelocity small radius unswept leading edges and nose-tips. NASA Technical Memorandum 1122204
3. Walker SP, Sullivan BJ (2003) Paper AIAA-2003-6915. Published in the proceedings of the 12th AIAA international space planes and hypersonic systems and technologies conference, American Institute of Aeronautics and Astronautics, Norfolk, VA, December 15–19
4. Levine SR, Opila EJ, Halbig MC, Kiser JD, Singh M, Salem JA (2002) J Eur Ceram Soc 22:2757

5. Chamberlain AL, Fahrenholtz WG, Hilmas GE, Ellerby DT (2004) J Am Ceram Soc 87:1170
6. Chamberlain AL, Fahrenholtz WG, Hilmas GE, Ellerby DT (2004) Key Eng Mater 493:264–268
7. Van Wie DM, Drewry DG Jr, King DE, Hudson CM (2004) J Mater Sci 39:5915
8. Monteverde F, Bellosi A (2003) J Electrochem Soc 150:B552
9. Monteverde F, Bellosi A, Guicciardi S (2002) J Eur Ceram Soc 22:279
10. Rieck U, Bolz J, Muller-Wiesner D (1995) Int J Mater Prod Tec 10:303
11. Kochendorfer R. International symposium for light weight structures proceedings, ESTEC, Noordwijk, The Netherland, 25–27 March, 1992 (ESA SP-336, October 1992), p 7
12. Fahrenholtz WG, Hilmas GE, Chamberlain AL, Zimmermann JW (2004) J Mater Sci 39:5951
13. Kuwabara K, Sakamoto S, Kida O, Ishino T, Kodama T, Nakajima H, Ito T, Hirakawa Y (2005) Proceedings of international conference on refractories, UNITECR'03, Osaka, Japan, p 302
14. Kinoshita S, Yoshimasa Y, Ono Y (2003) Proceedings of international conference on refractories, UNITECR'03, Osaka, Japan, p 205
15. Prietzel S, Hunold K, Potscke J, Kross U (2001) Proceedings of international conference on refractories, UNITECR'01, Cancun, Mexico, p 983
16. Kaji N, Shikano H, Tanaka I (1992) Taikabutsu Overseas 14:39
17. Norasetthekul S, Eubank PT, Bradley WL, Bozkurt B, Stucker B (1999) J Mater Sci 34:1261
18. Upadhya K, Yang J-M, Hoffman WP (1997) Am Ceram Soc Bull 58:51
19. Mroz C (1994) Am Ceram Soc Bull 73:141
20. Zhang G-J, Deng Z-Y, Kondo N, Yang J-F, Ohji T (2000) J Am Ceram Soc 83:2330
21. Goldstein A, Gefen Y, Goldenberg A (2001) J Am Ceram Soc 84:642
22. Zhang GJ, Ando M, Yang JF, Ohji T, Kanzaki S (2004) J Eur Ceram Soc 24:171
23. Nishida A, Shimamura T, Kohtoku Y (1990) J Ceram Soc Jpn 98:412
24. O YT, Koo JB, Hong KJ, Park JS, Shin DC (2004) Mater Sci Eng A 374:191
25. Koyama T, Nishiyama A, Niihara K (1994) J Mater Sci 29:3949
26. Mishra SK, Das SK, Ray AK, Ramachandrarao P (2002) J Am Ceram Soc 85:2846
27. ASTM C 1259-01 (2005) ASTM book of standards. ASTM International, West Conshohocken, PA
28. ASTM C 1161-02c (2005) ASTM book of standards. ASTM International, West Conshohocken, PA
29. Chantikul P, Anstis GR, Lawn BR, Marshall DB (1981) J Am Ceram Soc 64:539
30. Wachtman JB (1996) Mechanical properties of ceramics. John Wiley & Sons Inc., New York
31. Chamberlain AL, Fahrenholtz WG, Hilmas GE (2006) J Am Ceram Soc 89:450
32. Cutler RA (1991) In: Schneider SJ Jr (ed) Ceramics and glasses, engineered materials handbook, vol 4. ASM International, Materials Park, OH, p 787
33. Shaffer PTB (1991) In: Schneider SJ Jr (ed) Ceramics and glasses, engineered materials handbook, vol 4. ASM International, Materials Park, OH, p 804
34. Ohji T, Jeong Y-K, Chao Y-H, Niihara K (1998) J Am Ceram Soc 81:1453
35. Wiederhorn SM (1984) Annu Rev Mater Sci 14:374
36. Ruhle M, Dalgleish BG, Evans AG (1987) Scr Metall Mater 21:681
37. Rice RW (1981) Ceram Eng Sci Proc 2:661
38. Rice RW (1985) Ceram Eng Sci Proc 6:589